Coverage Enhancement of Underwater Internet of Things Using Multilevel Acoustic Communication Networks

Jiajie Xu, *Student Member, IEEE*, Mustafa A. Kishk, *Member, IEEE*, and Mohamed-Slim Alouini, *Fellow, IEEE*

***Abstract*—Underwater acoustic communication networks (UACNs) are considered a key enabler to the Underwater Internet of Things (UIoT). UACN is regarded as essential for various marine applications, such as monitoring, exploration, and trading. However, a large part of existing literature disregards the 3-D nature of the underwater communication system. In this article, we propose a *K*-tier UACN that acts as a gateway that connects the UIoT with the space–air–ground–sea integrated system (SAGSIS). The proposed network architecture consists of several tiers along the vertical direction with adjustable depths. On the horizontal dimension, the best coverage probability (CP) is computed and maximized by optimizing the densities of surface stations (SSs) in each tier. On the vertical dimension, the depth of each tier is also optimized to minimize intertier interference and maximize overall system performance. Using tools from stochastic geometry, the total CP of the proposed *K*-tier network is analyzed. For given spatial distribution of UIoT device's depth, the best CP can be achieved by optimizing the depths of the transceivers connected to the SSs through a tether. We verify the accuracy of the analysis using Monte Carlo simulations. In addition, we draw multiple useful system-level insights that help optimize the design of underwater 3-D networks based on the given distribution of UIoT device's depths.**

***Index Terms*—Coverage probability (CP), *K*-tier network, stochastic geometry, underwater communication, Underwater Internet of Things (UIoT).**

I. Introduction

OWING to the recent advances in wireless communication technology, space–air–ground–sea integrated systems (SAGSIS) is envisioned as a key player in the next-generation of wireless networks. As a part of SAGSIS in underwater, the Underwater Internet of Things (UIoT) is a carrier that promotes the development of underwater applications, such as high-speed marine communication which can provide a global connection for underwater devices [1], sea gilders which can be used for marine environmental monitoring, underwater drone clusters which can be used for underwater terrain exploration or mapping [2], and underwater sensor and communication systems for target detection and tracking [3], to name a few. In terms of underwater network, along with the marine technology sector and ocean development, like the research about marine environmental information monitoring and data acquisition UIoT in [4], [5], underwater communication networks has been developing rapidly and attracted the attention of many researchers. Underwater acoustic communication networks (UACNs) can be regarded as one of the basic infrastructures of an underwater system, especially in a large-scale system [6]. Although radio frequency (RF) and visible light communication (VLC) can also be used, their limited propagation distance makes them less favorable in underwater environments compared to acoustic communication [7], [8], [9]. Communication and information exchange among devices in the underwater environment is necessary for various purposes, such as localization, detection, and energy optimization, to name a few [10], [11], [12], [13]. Connectivity of underwater networks is also vital for some applications such as autonomous underwater vehicles (AUVs) [14].

In this article, we design a cross-medium network that can be regarded as the gateway between space–air–ground integrated networks and the underwater wireless networks, and which can provide a broader prospect for the development of underwater communication networks and the UIoT. We consider a *K*-tier UACN where each tier is placed at a different level and represents a set of surface stations (SSs) that is extending their transceivers/receivers to a unique depth using a tether. For that setup, we focus on the coverage probability (CP) analysis and the optimal values of such tethers for a given distribution of UIoT devices. More details regarding the contributions of this article are provided later in this section.

A. Related Work

In this section, we provide a brief summary of the related works in three general directions of interest to this article: 1) modeling and analysis of UACNs and UAWSNs; 2) stochastic geometry-based analysis of underwater communications; and 3) the related works on CP of UIoT.

Modeling and Analysis of UACNs and UAWSNs: A common practice in literature is to model the underwater communication networks as a 2-D network, which disregards the depth of

Manuscript received 17 February 2022; accepted 25 July 2022. Date of publication 3 August 2022; date of current version 7 December 2022. This work was supported by KAUST Office of Sponsored Research. *(Corresponding author: Mustafa A. Kishk.)*

Jiajie Xu and Mohamed-Slim Alouini are with the Computer, Electrical, and Mathematical Science and Engineering Division, King Abdullah University of Science and Technology, Thuwal 23955, Saudi Arabia (e-mail: jiajie.xu.1@kaust.edu.sa; slim.alouini@kaust.edu.sa).

Mustafa A. Kishk is with the Department of Electronic Engineering, Maynooth University, Maynooth, W23 F2H6 Ireland (e-mail: mustafa.kishk@mu.ie).

Digital Object Identifier 10.1109/JIOT.2022.3196180

different nodes and UIoT devices [15], [16]. However, there are also few works that considered a 3-D model for the underwater network. For instance, Jin *et al.* [17] proposed a 3-D network that is built by depth-adjustable nodes, i.e., every node can choose its depth freely. The authors also assumed that the initial 2-D coordinates of all the depth-adjustable nodes are known and fixed. Su *et al.* [18] used a similar network model and aimed to reduce the overlap between close nodes by adjusting the depth of nodes. One important aspect of UACNs that requires careful modeling is interference. Due to the use of omnidirectional communication nodes, interference can not be ignored and it can actually lead to a reduction in the communication distance of network nodes and consequently in CP. In [19], the overlapping coefficient "buoy group" mode is proposed. For a 2-D network model, the randomness in the locations of underwater targets and interference are considered.

Stochastic Geometry-Based Analysis of Underwater Communications: Stochastic geometry is becoming a powerful tool for network performance analysis [20], [21], [22]. In the underwater area, there are rare works that utilize this tool, despite its tractability and the fact that it fits well random nature of the underwater environment. To the best of our knowledge, the only paper related to stochastic geometry in underwater is [23]. In this article, a cluster-based underwater wireless sensor network is proposed. The network is divided into several small clusters and each cluster has only one head that can collect the information from its members and forward it to surface nodes. The locations of all the sensors or nodes are modeled as a homogeneous Poisson point process (PPP). The cluster-based network is a distributed 2-D network, while the influence of the distribution of depth of UIoT device on the performance is not captured. In addition, Rayleigh fading is considered for the channel model, which is impractical for the underwater scenario.

Works Related to CP of UIoT: Few works are focused on the issue of enhancement of CP of UIoT. In [24], the connectivity and CP are analyzed based on the underwater cognitive acoustic networks, primary users, and secondary users are designed to avoid the communication collision. However, the features of 3-D underwater space, like the random distribution of the UIoT devices and interference from different network nodes, are not taken into account. In [25], the system structure and open issues of UIoT are discussed, and AUV, smart sensors, etc., are clarified to be included in the future.

B. Contributions

This article provides one of the first attempts to model the underwater communication network using tools from stochastic geometry while using a realistic model for the communication channel. The analysis and optimization of CP of a 3-D UACN are provided based on a new K-tier network model. The main contributions of this article are listed as follows.

1) *We Design a New Multitier UACN Model Which Has a Cross-Medium Structure:* In order to extend the applications of UIoT and SAGSIS, a K-tier UACN with surface buoy receiver which can communicate with the stations in air or space (UAV, HAP, satellite, etc.) and underwater transmitter/receiver with adjustable depth is proposed. Besides that, a detailed analysis of the CP is made.
2) Considering the harshness of the underwater environment, it is almost impossible to make any assumptions about the location of the SSs and the randomness of the UIoT devices, we propose to use a random PPP to describe the deployment of SSs and UIoT devices. Due to the influence of ocean currents and waves, added to the weakness of the global position system (GPS), the positions of SSs and UIoT devices are almost random, so, we prefer a PPP to model the locations of the SSs and the UIoT devices.
3) *Optimal K-Tier Network for a Given UIoT Device's Depth Distribution:* Subject to a constraint on the density of SSs in the UACN system, we analyze and optimize the CP by adjusting the different tiers' tether lengths. Using numerical results, we draw multiple useful systems insights that can be helpful in designing efficient UIoT networks.

The rest of the manuscript is organized as follows. Section II describes the system model of the proposed K-tier UACN. Section III gives the detailed mathematical derivation of the CP. Section IV verifies the correctness of theoretical analysis compared with the Monte Carlo simulations, discloses the insights of the K-tier UACN, and provides solutions to maximize the CP of UIoT. Conclusions and future work are stated in Section V.

II. System Model

In this section, we propose a new structure for a K-tier underwater acoustic network, which is described in Fig. 1. In the K-tier network model, we have a set of SSs, each composed of a surface buoy and an underwater antenna, where the buoy and the antenna are linked by a tether. The locations of the SSs are modeled by k different PPPs, $\Phi_1, \Phi_2, \ldots, \Phi_k$ with densities $\gamma_1, \gamma_2, \ldots, \gamma_k$. The SSs in each tier j has the same tether length t_j. Each SS is annotated as $S_{j,i}$, with $j = 1, 2, \ldots, K$, indicating which tier the SS belongs to, and $i = 1, 2, \ldots,$ indicates the SS is the ith nearest SS to the reference UIoT device from the jth tier. In Fig. 1, an example of the considered setup is provided. Cartesian coordinates $(x_{j,i}, y_{j,i}, t_j)$ are used to model the locations of UIoT devices or the transceivers, where t_j is the tether length of jth tier.

Besides stations, we also have different UIoT devices, like AUVs or sensor nodes as shown in Fig. 1. We model the locations of the UIoT devices at a given depth as a PPP. We consider a reference UIoT device at depth u_r. The coordinates of the reference UIoT device are $U_r = (x_r, y_r, u_r)$. Given that the locations of SSs and the UIoT devices are horizontally distributed according to two independent PPPs, the stationarity of the PPP, and according to the Slyvniak's theorem, we can always focus on the performance of a "typical" UIoT device located at the origin without loss of generality [26], [27].

Definition 1: Distance between a SS and an UIoT device is

$$D_{S_{j,i}\to U_r} = \sqrt{\left(x_{j,i} - x_r\right)^2 + \left(y_{j,i} - y_r\right)^2 + \left(t_j - u_r\right)^2} \quad (1)$$

TABLE I
DEFINITIONS OF SONAR'S PARAMETERS AND REFERENCE LOCATIONS

Parameter	Definition
Source Level, SL	$10\times \log \frac{Signal\ strength\ at\ one\ meter}{Reference\ strength}$
Transmit Loss, TL	$10\times \log \frac{Signal\ strength\ at\ one\ meter}{Signal\ strength\ at\ the\ receiver}$
Noise Level, NL	$10\times \log \frac{Noise\ strength}{Reference\ strength}$
Directivity Index, DI	$10\times \log \frac{Output\ noise\ power\ of\ non-directional\ hydrophone\ strength}{Output\ noise\ power\ of\ directional\ hydrophone\ strength}$

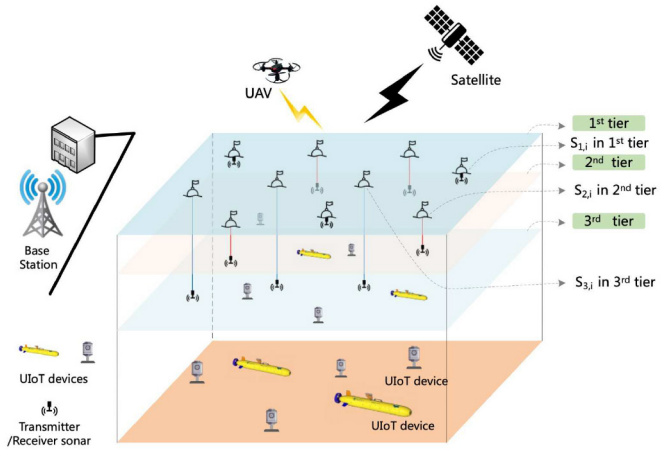

Fig. 1. Diagram of the underwater acoustic K-tier network.

where j means the order of the tiers and i means the order of the points in the tier. Without loss of generality, we assume that the UIoT device projection position is directly at the origin. Hence, the distance can be rewritten as $D_{S_{j,i}\to U_r} = \sqrt{r_{j,i}^2 + (t_j - u_r)^2}$ where $r_{j,i}^2 = x_{j,i}^2 + y_{j,i}^2$, and in the following we will regard $D_{S_{j,i}\to U_r}$ as $D_{j,i}$ for simplicity.

Before we discuss the underwater channel model, it is worth mentioning that an accurate model should take into consideration the sea depth, temperature, and salinity level. The model used in this article is a semi-empirical model that was first proposed [28] based on multiple experiments and is currently widely used in [29], [30], and [31].

A. Underwater Acoustic Communication Channel

The power received at the reference UIoT device from a given transmitter is

$$\mathrm{PR} = \mathrm{SL} - \mathrm{TL} - (\mathrm{NL} - \mathrm{DI}) \tag{2}$$

where PR is the power received which can be regarded as received signal power, SL is the source level which is the transmission power, TL is the transmission loss, NL is the noise level, DI is the directivity index, and the units of all these quantities are the same, dB. We have the definitions as shown in Table I, and in this table, the *Reference strength* is the plane wave sound strength with a root mean square sound pressure of 1 μpa [28]. We can compute SL in dB as follows:

$$\mathrm{SL} = 10\log\frac{P_t/4\pi}{\text{Reference strength}} = 10\log\frac{P_t/4\pi}{10^{-12}/1.5\times 10^6}$$
$$= 10\log P_t + 10\log\frac{1.5\times 10^{18}}{4\pi} \approx 10\log P_t + 170.77 \tag{3}$$

where P_t is the signal power of transmission with the unit of watts. So In the same way, we can also get

$$\begin{cases} \mathrm{TL} = 10\times\log(T_l) + 170.77\ (\mathrm{dB}) \\ \mathrm{NL} = 10\times\log(N_l) + 170.77\ (\mathrm{dB}) \\ \mathrm{DI} = 10\times\log(D_i) + 170.77\ (\mathrm{dB}) \\ \mathrm{PR} = 10\times\log(P_r) + 170.77\ (\mathrm{dB}) \end{cases} \tag{4}$$

where T_l is the transmission loss, N_l is the noise, D_i is the direct gain, and P_r is the received signal power, all in watts.

According to (3) and (4), the received signal power P_r can be derived as follows:

$$10\log\frac{1.5\times 10^{18}P_r}{4\pi} = 10\log P_t - 10\log T_l - 10\log N_l + 10\log D_i$$
$$= 10\log\frac{P_t\times D_i}{T_l\times N_l}. \tag{5}$$

If we transfer the unit dB into watts, (5) can be written as

$$P_r = \frac{4\pi P_t\times D_i}{1.5\times 10^{18}T_l\times N_l}. \tag{6}$$

B. Underwater Acoustic Path Loss

In general, there are two factors of energy loss during the propagation of acoustic waves in water, *Geometric Spreading Loss* and *Attenuation Loss*. Both of these two types of power loss mainly depend on distance and frequency of propagation.

1) Geometric Spreading Loss: The geometric spreading loss means a geometric effect that regularly weakens the sound wave as it expands outward from the sound source. Spreading loss increases with distance, and changes with distance logarithmically. Spreading loss η can be divided into three different types; 1) spherical spreading loss η_s; 2) cylindrical spreading loss η_c; and 3) mixed spreading loss η_m. Cylindrical spreading loss η_c should be used when the communication distance d is much longer than the distance r between the upper and lower boundaries, and the spherical spreading loss η_s should be applied when d is equal to or less than r, otherwise mixed spreading loss η_m should be used. Geometric spreading loss can be shown as

$$\eta = \lambda\times 10\log(1000d) \tag{7}$$

where d with the unit of km means propagation distance between a pair of SS and UIoT devices, and generally λ is a constant which equals 1.5 in common underwater application scenarios.

2) Attenuation Loss: Attenuation loss includes absorption, scattering, and acoustic energy leakage. However, absorption loss and scattering loss are difficult to distinguish, so they

are generally calculated together. The loss of sound energy is usually small, so the loss is generally ignored.

The overall transmission loss that captures all factors can be written as follows:

$$\mathrm{TL} = \eta + \alpha(f)d \tag{8}$$

where η is geometric spreading loss with unit dB, d is the distance between two nodes with unit km, f is the transmission frequency, $\alpha(f)$ is the absorption coefficient with unit dB/km, and it can be also written with units of dB

$$10\log\left(\frac{1.5\times 10^{18}T_l}{4\pi}\right) = 10\lambda\log(1000d) + \alpha(f)d. \tag{9}$$

We can also convert TL from dB into absolute value, and we can get

$$T_l(\lambda, f, d) = \beta(\lambda)d^{\lambda}10^{0.1\alpha(f)d} \tag{10}$$

where $\beta(\lambda) = ((4\pi 10^{3\lambda})/(1.5\times 10^{18}))$. According to Thorp's formula [32], the following α can be used as a simplified model for frequencies less than 50 kHz:

$$\alpha(f) = \frac{0.11f^2}{1+f^2} + \frac{44f^2}{4100+f^2} + 2.75\times 10^{-4}f^2 + 0.003. \tag{11}$$

Since λ, f, D_i, and N_l are known in advance, $\beta(\lambda)$ and $\alpha(f)$ are calculated as constants, we can rewrite P_r as

$$P_r(d) = \frac{P_t}{C\times Tl(\lambda, f, d)} \tag{12}$$

where $C = (1000^{\lambda}N_l/D_i)$ is a constant, $Tl(\lambda, f, d) = d^{\lambda}10^{0.1\alpha(f)d}$, and we will write $Tl(\lambda, f, d)$ as $Tl(d)$ for simplicity.

C. Communication Link in K-Tier Network

We assume the nearest SS association policy, namely, the UIoT device associates with the nearest SS (the nearest transceiver). The signals incoming from the rest of the SSs are regarded as interference. Hence, it is essential to calculate the signal-to-interference and noise ratio (SINR) to determine whether the received useful signal P_r can be recognized by the particular UIoT device. Combine with threshold τ, the CP of the SS to the UIoT device can be written as

$$P_{\mathrm{cov}}(\lambda, f, d) = \mathbb{P}[\mathrm{SINR} > \tau] = \mathbb{P}\left[\frac{P_r}{\sigma^2 + I_R} > \tau\right] \tag{13}$$

where σ^2 is the variance of Gaussian white noise (GWN), I_R is the interference, and τ is the threshold of the received SINR to enable signal decoding. To compute the CP, we need the distribution of P_r and I_R. To calculate the distribution of P_r, we need to derive the distribution of the distance to the closest SS. Combined with underwater acoustic channel signal propagation loss, we can obtain the distribution of path loss of the closest distance. As for interference in the K-tier network, it can be divided into two parts: 1) interference created by SSs in the same tier with the tagged SS and 2) interference made by SSs in other tiers.

If the nearest SS belongs to the mth tier, the distance between the reference UIoT device and this SS is $D_{m,1}$. So, with the given u_r we have the following definition.

Definition 2: The CP of a K-tier network is

$$\mathbb{P}[\mathrm{SINR} > \tau|u_r] = \sum_{m=1}^{k} A_m\mathbb{P}[\mathrm{SINR}_m > \tau|u_r] \tag{14}$$

where A_m is the mth tier association probability, which means the probability that the closest SS belongs to the mth tier, and

$$\mathbb{P}[\mathrm{SINR}_m > \tau|u_r] = \mathbb{P}\left[\frac{P_r(m)}{\sigma^2 + I_{\mathrm{Intra}-m} + I_{\mathrm{Inter}}} > \tau\middle|u_r\right] \tag{15}$$

where $P_r(m)$ is received signal power when the UIoT device is associated with the mth tier. According to (10) and (12), the received useful signal can be written as

$$P_r(m|u_r) = \frac{P_t}{C}Tl^{-1}\left(D_{m,1}|u_r\right) \tag{16}$$

where $D_{m,1}$ means the distance between the nearest SS in mth tier to the target UIoT device. Besides that, we sort all the distances between the target UIoT device and the SSs in a tier, so $D_{m,1}$ means the shortest distance to the target UIoT device in the mth tier.

For the interference, we divided them into intrainterference which is in the same tier as the useful signal, and interinterference which is in other tiers, and they are shown as

$$I_{\mathrm{Intra}-m}\left(D_{m,i}|u_r\right) = \sum_{i=2}\left(\frac{P_t}{C}Tl^{-1}\left(D_{m,i}|u_r\right)\right) \tag{17}$$

$$I_{\mathrm{Inter}}\left(D_{j,i}|u_r\right) = \sum_{j=1, j\neq m}^{k}\sum_{i=1}\left(\frac{P_t}{C}Tl^{-1}\left(D_{j,i}|u_r\right)\right). \tag{18}$$

III. Mathematical Analysis of Coverage Probability

Recall that we have the transmission loss as a function of the distance d, $Tl(d) = \beta d^{\lambda}10^{0.1\alpha(f)d}$. In this section, we will derive the distribution of the received signal power when associating with the mth tier, the distribution of the interference created by SSs in the mth tier, and the distribution of interference created by SSs in other tiers, and the associate probability.

A. Distributions of Distance and Path Loss

In a PPP, the probability density function (PDF) of the distance from a reference location located at the origin o to the nth nearest point is [33]

$$f(r, n) = \frac{2(\pi\gamma)^n}{(n-1)!}r^{2n-1}\exp\left(-\pi\gamma r^2\right),\ \ r > 0, n = 1, 2, \ldots \tag{19}$$

where γ is the density of the PPP.

Recall that due to the memoryless property of the Poisson process the above equation applies for any arbitrary location to its nth nearest point, i.e., does not have to be at the origin.

In the following, for simplicity and without any ambiguity, we will use $f(r_1), f(r_2)$ to donate $f(r,1)$ and $f(r,2)$, so we have

$$f(r_1) = 2\pi\gamma r \exp\left(-\pi\gamma r^2\right) \tag{20}$$

$$f(r_2) = 2(\pi\gamma)^2 r^3 \exp\left(-\pi\gamma r^2\right). \tag{21}$$

1) Distributions of Closest Distance and Path Loss in Every Tier: In order to calculate the CP in the K-tier network, we first compute the distribution of the distance between the reference UIoT device and the nearest SS in each tier. The horizontal distance (distance between projections on x–y plane) between the reference UIoT device and the closest SS in the jth tier is annotated as $R_{j,1}$ where $D_{j,1} = \sqrt{R_{j,1}^2 + z_j^2}$ and z_j is relative depth which is $z_j = t_j - u_r$. The cumulative distribution function (CDF) of $R_{j,1}$ is $F_{R_{j,1}}(r_{j,1}) = 1 - \exp(-\gamma_j \pi r_{j,1}^2)$ and the PDF can be found as

$$f_{R_{j,1}}(r_{j,1}) = \frac{\mathrm{d}F_{R_{j,1}}(r_{j,1})}{\mathrm{d}r_{j,1}} = 2\pi\gamma_j r_{j,1} \exp\left(-\gamma_j \pi r_{j,1}^2\right). \tag{22}$$

With the CDF of $R_{j,1}$ in (22), and given that $R_{j,1}$ must bigger than the relative depth $|z_j|$, we get

$$\begin{aligned} F_{D_{j,1}}(d_{j,1}) &= P(D_{j,1} \le d_{j,1}) \\ &= P\left(\sqrt{R_{j,1}^2 + z_j^2} \le d_{j,1}\right) \\ &= P\left(0 \le R_{j,1} \le \sqrt{\max\left(d_{j,1}^2, z_j^2\right) - z_j^2}\right) \\ &= 1 - \exp\left(-\gamma_j \pi \left(\max\left(d_{j,1}^2, z_j^2\right) - z_j^2\right)\right). \end{aligned} \tag{23}$$

Differentiation with respect to $d_{j,1}$, we have the PDF of $D_{j,1}$ as follows:

$$f_{D_{j,1}}(d_{j,1}) = \begin{cases} 2\pi\gamma_j d_{j,1} \exp\left(-\gamma_j \pi \left(d_{j,1}^2 - z_j^2\right)\right), & \text{if } d_{j,1}^2 > z_j^2 \\ 0, & \text{else.} \end{cases} \tag{24}$$

2) Distribution of the Distance to the Nearest SS Conditioned on the Distance to the Second Nearest SS: The distribution of $R_{j,2}$ conditioned on $R_{j,1}$ is a well-known result in [34], which is

$$f(r_{j,2}|r_{j,1}) = 2\gamma_j \pi r_{j,2} \exp\left(-\gamma_j \pi \left(r_{j,2}^2 - r_{j,1}^2\right)\right) \tag{25}$$

$$\begin{aligned} f(r_{j,1}, r_{j,2}) &= f(r_{j,1}) f(r_{j,2}|r_{j,1}) \\ &= f(r_{j,2}) f(r_{j,1}|r_{j,2}) \\ &= (2\gamma_j \pi)^2 r_{j,1} r_{j,2} \exp\left(-\gamma_j \pi r_{j,2}^2\right) \end{aligned}$$

$$f(r_{j,1}|r_{j,2}) = \frac{f(r_{j,1}, r_{j,2})}{f(r_{j,2})} = \frac{2r_{j,1}}{r_{j,2}^2}. \tag{26}$$

B. Distribution of the Received Power From the Tagged SS in the mth Tier

When the tagged SS is in mth tier and the probability that $\mathrm{SINR_m}$ bigger than the threshold is shown in (15), here we give the definition of distribution of the useful signal.

Definition 3: The CP is described in Definition 2, and we have useful signal power $P_r(m|u_r) = (P_t/C) Tl_{D_{m,1}}^{-1}(d_{m,1}|u_r)$, where $Tl^{-1}(d_{m,1}|u_r)$ is the path loss of useful signal. So, we need to calculate the distribution of path loss. In order to make the calculation more simple, we make a definition that

$$Tl^{-1}(D_{m,1}|u_r) = D_{m,1}^{-\lambda} 10^{-0.1\alpha D_{m,1}} \triangleq Y_{m,1}. \tag{27}$$

So, in the following, we need to derive the distribution of $Y_{m,1}$.

Lemma 1: Using (26), we can get the CDF of $D_{m,1}$

$$\begin{aligned} F_{D_{m,1}}(d_{m,1}|r_{m,2}) &= P(D_{m,1} \le d_{m,1}|r_{m,2}) \\ &= \frac{\min\left(\max\left(d_{m,1}^2 - (u_r - t_m)^2, 0\right), r_{m,2}^2\right)}{r_{m,2}^2} \end{aligned} \tag{28}$$

where $d_{m,1}^2 = r_{m,1}^2 + (u_r - t_m)^2$.

Proof: See Appendix A. ∎

Before we compute the distribution of $Y_{m,1}$, we need to introduce an important rule that the inverse of the function $y = x^{-a} 10^{-bx}$ can be written as

$$x = \frac{aW\left(\frac{b}{a}\left(y \ln^{-a}(10)\right)^{\frac{-1}{a}}\right)}{b \ln(10)} \tag{29}$$

where $W(\cdot)$ means Lambert W function.

So we can get the inverse function of $y_{m,1} = d_{m,1}^{-\lambda} 10^{-0.1\alpha d_{m,1}}$ as following:

$$d_{m,1} = \frac{10\lambda}{\alpha \ln(10)} W\left(\frac{\alpha \ln(10)}{10\lambda} y_{m,1}^{\frac{-1}{\lambda}}\right). \tag{30}$$

As we can see that

$$\frac{\partial Y_{m,1}}{\partial D_{m,1}} = -10^{-0.1\alpha D_{m,1}} \left(\lambda D_{m,1}^{-\lambda-1} + \alpha D_{m,1}^{-\lambda} \frac{\ln 10}{10}\right) \tag{31}$$

is always a nonpositive value, so $Tl^{-1}(D_{m,1})$ is a monotonically decreasing function.

Lemma 2: So, we can get the distribution of $Y_{m,1}$ conditioned on $r_{m,2}$

$$\begin{aligned} F_{Y_{m,1}}(y_{m,1}|r_{m,2}) &= P(Y_{m,1} \le y_{m,1}|r_{m,2}) \\ &= 1 - \frac{\min\left(\max\left(\left(\frac{10\lambda}{\alpha \ln(10)} W\left(\frac{\alpha \ln(10)}{10\lambda} y_{m,1}^{\frac{-1}{\lambda}}\right)\right)^2 - (u_r - t_m)^2, 0\right), r_{m,2}^2\right)}{r_{m,2}^2}. \end{aligned} \tag{32}$$

Proof: See Appendix B. ∎

The above distribution is essential for the computation of the CP, as will be shown later.

C. Distributions of Interference in the mth Tier and Other Tiers

According to (15), we divide the interference into two parts: 1) intrainterference which is the interference coming from the SSs in the mth tier and 2) interinterference which is made by SSs in other tiers. In the following, we will compute distributions of them, respectively. In the following, we define $I_{\mathrm{Intra}-m}$ as the intrainterference in mth tier and I_{Inter} as the interinterference.

1) Interference From SS in the mth Tier:

Definition 4: Here, we give the definition of the intrainterference, and it can be divided into two parts, one is from the second nearest SS in mth tier, and the other part is coming from the rest of the SSs in the mth tier. The intrainterference can be written as

$$I_{\text{Intra}-m}(D_{m,i}|u_r) = \frac{P_t}{C} Tl^{-1}(D_{m,2}|u_r) + I_{\text{Intra}-m3}$$

where $I_{\text{Intra}-m3}(D_{m,i}|u_r) = \sum_{i=3}(P_t/C)Tl^{-1}(D_{m,i}|u_r)$.

Lemma 3: The expected value of $I_{\text{Intra}-m3}(D_{m,i}|u_r)$ is

$$\begin{aligned}\mathbb{E}\left[I_{\text{Intra}-m3}(D_{m,i}|u_r)\right] &= \mathbb{E}\left[\sum_{i=3} \frac{P_t}{C} Tl^{-1}(D_{m,i}|u_r)\right] \\ &= \frac{P_t}{C}\gamma_m 2\pi \left(\frac{1}{0.1\alpha}\right)^{2-\lambda} \ln^{\lambda-2}(10) \\ &\quad \times \Gamma\left(2-\lambda, \frac{\alpha D_{m,2}\ln(10)}{10}\right) \quad (33)\end{aligned}$$

where $\Gamma(\cdot)$ is a Gamma function, and as we can see that the expectation of the distribution of $I_{Inter-m3}$ is a function of $D_{m,2}$.

Proof: See Appendix C. ∎

Hence, the intrainterference conditioned on $R_{m,2}$ can be approximated as follows:

$$\begin{aligned}I_{\text{Intra}-m}(D_{m,2}|u_r) &= \frac{P_t}{C} D_{m,2}^{-\lambda} 10^{-0.1\alpha D_{m,2}} + \frac{P_t}{C}\gamma_m 2\pi \left(\frac{1}{0.1\alpha}\right)^{2-\lambda} \\ &\quad \times \ln^{\lambda-2}(10)\Gamma\left(2-\lambda, \frac{\alpha D_{m,2}\ln(10)}{10}\right) \quad (34)\end{aligned}$$

where $D_{m,2} = (R_{m,2}^2 + (u_r - t_m)^2)^{1/2}$.

2) Interference From the Rest of the Tiers:

Definition 5: The interference at the UIoT device coming from all the tiers except the mth tier is

$$I_{\text{Inter}}(D_{j,i}|u_r) = \sum_{j=1, j\neq m}^{k} I_{\text{Inter}-j}(D_{j,i}|u_r)$$

where the interference from jth tier is

$$\begin{aligned}I_{\text{Inter}-j}(D_{j,i}|u_r) &= \sum_{i=1}\left(\frac{P_t}{C} Tl^{-1}(D_{j,i}|u_r)\right) \\ j &= 1, 2, \ldots, k, t \neq m.\end{aligned}$$

In order to compute the distribution of interinterference in jth tier, we separate it into two parts, the first part is coming from the closest interferer at distance $D_{j,1}$ in every tier, while the second part is the interference coming from the rest of the SSs as follows:

$$I_{\text{Inter}-j}(D_{j,i}|u_r) = \frac{P_t}{C} Tl^{-1}(D_{j,1}|u_r) + I_{\text{Inter}-j2}(D_{j,i}|u_r) \quad (35)$$

where $I_{\text{Inter}-j2}(D_{t,i}|u_r) = \sum_{i=2}((P_t/C)Tl^{-1}(D_{j,i}|u_r))$.

Defining $Y_{j,1} = Tl^{-1}(D_{j,1}|u_r)$, similar to the previous section, we get

$$D_{j,1} = \frac{10\lambda}{\alpha\ln(10)} W\left(\frac{\alpha\ln(10)}{10\lambda} Y_{j,1}^{\frac{-1}{\lambda}}\right). \quad (36)$$

Lemma 4: The CDF of path loss $Y_{j,1} = Tl^{-1}(D_{j,1}|u_r)$ can be written as

$$F_{Y_{j,1}}(y_{j,1}) = \exp\left(-\gamma_j\pi\left(\left(\frac{10\lambda}{\alpha\ln(10)} W\left(\frac{\alpha\ln(10)}{10\lambda} y_{j,1}^{\frac{-1}{\lambda}}\right)\right)^2 - z_j^2\right)\right) \quad (37)$$

where $z_j^2 = (u_r - t_j)^2$.

Proof: See Appendix D. ∎

Define $\mathcal{G}(y_{j,1}) = ([\alpha\ln(10)]/10\lambda) y_{j,1}^{(-1/\lambda)}$ then we have

$$\begin{aligned}&f_{Y_{j,1}}(y_{j,1}) \\ &= \frac{2\gamma_j\pi 10 W(\mathcal{G}(y_{j,1}))}{\alpha\ln(10)\, y_{j,1}} \frac{\exp\left(-\gamma_j\pi\left(\left(\frac{10\lambda}{\alpha\ln(10)} W(\mathcal{G}(y_{j,1}))\right)^2 - z_j^2\right)\right)}{\frac{\alpha\ln(10)}{10\lambda} + y_{j,1}^{\frac{1}{\lambda}} \exp(W(\mathcal{G}(y_{j,1})))}. \quad (38)\end{aligned}$$

Lemma 5: After we have the distribution of the main interinterference in every tier, we need to calculate the expectation of the remaining interference

$$\begin{aligned}&\mathbb{E}\left[I_{\text{Inter}-j2}(D_{j,1}|u_r)\right] \\ &= \frac{P_t}{C}\gamma_j 2\pi \left(\frac{1}{0.1\alpha}\right)^{2-\lambda} \ln^{\lambda-2}(10)\Gamma\left(2-\lambda, \frac{\alpha D_{j,1}\ln(10)}{10}\right) \quad (39)\end{aligned}$$

where $\Gamma(\cdot)$ is the Gamma function.

Proof: See Appendix E. ∎

We can see that both $(P_t/C)Tl^{-1}(D_{j,1}|u_r)$ and $I_{\text{Inter}-j2}(D_{j,i}|u_r)$ are both functions of $D_{j,1}$ or $R_{j,1}$. So, with given u_r, we have the distribution of total interinterference as follows:

$$\begin{aligned}I_{\text{Inter}}(D_{j,1}, j = 1, 2, \ldots, k, j \neq m|u_r) &= \sum_{j=1, j\neq m}^{k} \left(\frac{P_t}{C} D_{j,1}^{-\lambda} 10^{-0.1\alpha D_{j,1}}\right. \\ &\quad \left. + \frac{P_t}{C}\gamma_j 2\pi \left(\frac{1}{0.1\alpha}\right)^{2-\lambda} \ln^{\lambda-2}(10)\Gamma\left(2-\lambda, \frac{\alpha D_{j,1}\ln(10)}{10}\right)\right) \quad (40)\end{aligned}$$

where $D_{j,1}^2 = R_{j,1}^2 + (u_r - t_j)^2$.

D. Association Probability

In this part, we will calculate the association probability which is the probability that the tagged SS is in the mth tier, and then we do a summation from $m = 1$ to $m = k$, to compute the CP.

Theorem 1: After we have CDF of the closest distance in every tier in (23), we assume that $D_{m,1}$ is the closest distance in $\{D_{j,1}|(R_{j,1}^2 + (u_r - t_j)^2)^{(1/2)}, j = 1, 2, 3, \ldots, k\}$ where $R_{j,1}^2 = x_{j,1}^2 + y_{j,1}^2$, so according to (23) we get the association probability with the mth tier A_m conditioned on u_r as follows:

$$\begin{aligned}A_{m|u_r} &= \prod_{j=1, j\neq m}^{j=k} \left(1 - \mathbb{1}(|u_r - t_m| < |u_r - t_j|)\frac{\gamma_j}{\gamma_j + \gamma_m}\right. \\ &\quad \times \exp\left(-\gamma_m\pi(u_r - t_j)^2 + \gamma_m\pi(u_r - t_m)^2\right) \\ &\quad + \mathbb{1}(|u_r - t_j| \leq |u_r - t_m|) \\ &\quad \left.\times\left(\exp\left(-\gamma_j\pi(u_r - t_m)^2 + \gamma_j\pi(u_r - t_j)^2\right) - 1\right)\right.\end{aligned}$$

$$- \mathbb{1}\left(|u_r - t_j| \le |u_r - t_m|\right)\frac{\gamma_j}{\gamma_j + \gamma_m} \times \exp\left(-\gamma_j \pi (u_r - t_m)^2 + \gamma_j \pi \left(u_r - t_j\right)^2\right)\Big| u_r\Big). \quad (41)$$

Proof: See Appendix F. ∎

Now we are ready to compute the CP, which is provided in the next section.

E. Coverage Probability

1) CP for Given Depth of UIoT Device u_r: The overall CP for a given value of u_r is given in the below theorem.

Theorem 2: The final expression of CP with given UIoT device's depth can be written as follows:

$$\mathbb{P}[\text{SINR} > \tau | u_r] = \sum_{m=1}^{k} A_m \mathbb{P}[\text{SINR}_m > \tau | u_r] \quad (42)$$

where A_m is shown in (41) and using (34) and (40), $\mathbb{P}[\text{SINR}_m > \tau | u_r]$ is

$$\mathbb{P}[\text{SINR}_m > \tau | u_r] = \int_{R_{m,2}} \int_{R_{1,1}} \int_{R_{2,1}} \cdots \int_{R_{k,1}} \left(1 - F_{Y_{m,1}}\left(y_{m,j} | r_{m,2}\right)\right) f\left(r_{1,1}\right) \times f\left(r_{2,1}\right) \cdots f\left(r_{k,1}\right) f\left(r_{m,2}\right) \mathrm{d}r_{1,1} \mathrm{d}r_{2,1} \cdots \mathrm{d}r_{k,1} \mathrm{d}r_{m,2}$$

where $f(r_{j,1})$ is shown in (22) and according to (21)

$$f\left(r_{m,2}\right) = 2\pi^2 \gamma_m^2 r_{m,2}^3 \exp\left(-\pi \gamma_m r_{m,2}^2\right)$$

and

$$1 - F_{Y_{m,1}}\left(y_{m,j} | r_{m,2}\right) = \frac{\left(\min\left(\sqrt{\max\left(\left(\frac{10\lambda}{\alpha \ln(10)} W\left(\frac{\alpha \ln(10)}{10\lambda} y_{m,j}^{\frac{-1}{\lambda}}\right)\right)^2 - (u_r - t_m)^2, 0\right)}, r_{m,2}\right)\right)^2}{r_{m,2}^2}$$

where

$$y_{m,j} = \tau \frac{C}{P_t}\Big(\sigma^2 + I_{\text{Intra}-m}\left(r_{m,2}\right) + I_{\text{Inter}}\left(r_{j,1}, j = 1, 2, \ldots, k, j \ne m\right)\Big| u_r\Big).$$

Proof: See Appendix G. ∎

2) Depth of UIoT Device u_r Subject to Given Distribution: We have calculated the CP of the K-tier network in (42) for a given UIoT device depth u_r. If the depth of the UIoT device follows a given probability distribution, we can regard u_r as a random variable instead of a constant with PDF $f_{U_r}(u_r)$. Therefore, the overall CP can be calculated by

$$\mathbb{P}[\text{SINR} > \tau] = \mathbb{E}_{U_r}[\mathbb{P}[\text{SINR} > \tau | u_r]]. \quad (43)$$

With a particular distribution of u_r, $\mathbb{P}[\text{SINR} > \tau]$ is only function of t_j and $\gamma_j, j = 1, 2, \ldots, k$.

Further, if we want to get the maximum CP $\mathbb{P}[\text{SINR} > \tau]$, we need to adjust the different tiers' tether lengths t_j under the constraint of the sum of the densities of PPPs γ_j in different tiers is constant. So, we can have the optimization problem as follows:

TABLE II
SETTING OF PARAMETERS IN SIMULATION

Parameter	Setting
Frequency, f	20 kHz
Geometric Expansion Factor, λ	1.5
Source Level, SL	180 dB
Directivity Index, DI	7.8 dB
Noise Level, NL	$115 - 20\log_{10}(f)$ dB
Gaussian White Noise, σ	10^{-6}

Algorithm 1 Calculate the CP in Simulation

Input: $f, \lambda, SL, DI, NL, \sigma, t_j, \gamma_j, \tau, u_r, n \leftarrow 0$;
Output: CP;
while $n <= iteration$ **do**
  $n \leftarrow n + 1$;
  Generate SSs according to PPP;
  Get the transmission distance from each SS to the origin;
  Calculate the desired signal power and the interference;
  Calculate SINR;
end while
CP = $\mathbb{P}[\text{SINR} > \tau]$;
return CP;

$$\max_{t_j, \gamma_j, j=1,2,\ldots,k} \mathbb{E}_{U_r}[\mathbb{P}[\text{SINR} > \tau | u_r]] \quad \text{s.t.} \sum_{j=1}^{j=k} \gamma_j = \Omega. \quad (44)$$

IV. Performance

In this section, we will verify the accuracy of the derived expression for the CP using Monte Carlo simulations. In addition, using single-tier and two-tier setups, we will try to reveal useful system-level insights, and the details of the simulation setup are shown in Table II. The pseudocode of the simulation process is shown in Algorithm 1, and it is executed on the simulation platform of MATLAB 2020a.

A. Single-Tier Network

The comparison between mathematical analysis and simulation for a single-tier network is shown in Fig. 2. In this comparison, we set the tether length as 2 km, and the density of the PPP is 2 SSs/km^2. The continuous curves and star curves are results of analysis and simulation under three different values of τ, respectively. We can see that the results of analysis and simulation are matching with a very small gap as a result of the approximation applied in the analysis of the interference.

Before proceeding with the rest of the simulation results, we define two useful metrics that can be used to analyze the performance of the considered system.

Definition 6: The range of CP is defined as the range of the UIoT device's depth, u_r, that can achieve a CP bigger than a predefined threshold. If the CP is smaller than the predefined threshold, we consider the coverage performance of the network to be unacceptable. The peak of CP is the

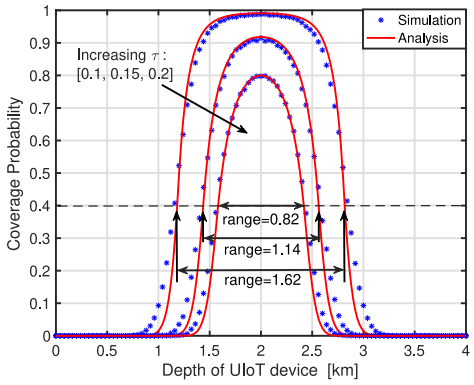

Fig. 2. CP of single-tier network with $t = 2$ km, $\gamma = 2$ SSs/km^2.

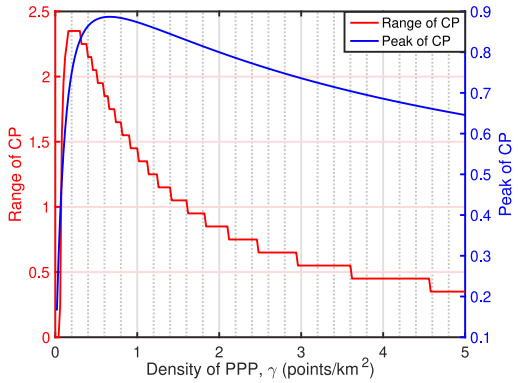

Fig. 3. Range and peak of CP in single-tier network with $\tau = 2$, $t = 5$ km.

biggest value that the CP can achieve for different values of u_r.

For example, we consider a scenario where this predefined threshold is 0.4. Hence, a CP below 0.4 is considered unacceptable. In that case, the range of CP is defined as the range of UIoT devices' depth that can achieve CP above 0.4. In Fig. 2 , we can see that the ranges of analysis result with $\tau = 0.1, 0.15, 0.2$ are 1.62, 1.14, and 0.82 km, respectively. It shows that if the detection threshold τ is smaller, the CP range is bigger, and this makes sense. In this figure, it is also easy to find that the tether length t may not affect the range but the density of PPP γ has a significant influence. Besides that, we can find that the peak of each curve is achieved when the tether length is equal to the depth of the UIoT device, which is 2 km. It means that when the UIoT device is set at the same level as the SSs, the CP is maximized. While these results are trivial, they become more complicated as we proceed to the multitier scenario in the next part.

In Fig. 3 , we provide the values of the range and peak for different values of γ with $\tau = 0.2$, $t = 5$ km and the depth of u_r vary from 0 to 10 km. In this figure, we can find that when the $\gamma = 0.6$ SSs/km^2, the peak will achieve the biggest value, and when the $\gamma = 0.3$ SSs/km^2, the range will be the biggest. Those two results are very useful when we design our underwater communication K-tier network and decide which γ we should choose.

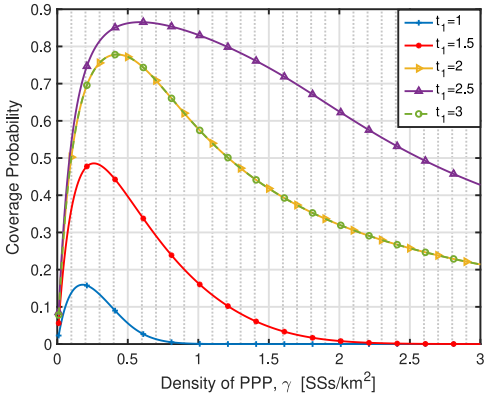

Fig. 4. Range and peak of CP in single-tier network with different densities of PPPs with $\gamma = 2$ SSs /km^2.

In Fig. 4, we have five different curves, each representing a different tether length from 1 to 3 km. For each of these values, we plot the CP for different values of γ. It should be clarified that the detect threshold τ is 0.2, and the UIoT device's depth is subject to a uniform distribution over [2, 3] km. In Fig. 4, we can find that on each curve, there is a peak, at where the density of PPP we should choose in our design, and the peak of each curve is unique, which means that if we decide on a tether length, the peak points to the optimal γ that should be used. Besides that, we can see the curves representing the length of the tether 2 and 3 km, respectively, are coincident. This is because the UIoT device's depth is subject to a uniform distribution over [2, 3] km. When the length of the tether is 2 km, the single-tier network is at the upper edge of the area where the UIoT devices are distributed. When the length of the tether is 3 km, the single-tier network is at the lower edge of the area where the UIoT devices are distributed. Since the UIoT device locations are uniformly distributed both horizontally over [2, 3] km and vertically, both scenarios are identical in terms of CP performance.

In Fig. 5, we study the influence of the tether length on the CP for two different distributions of UIoT device depth. In particular, we set the UIoT device's depth subject to a uniform distribution over [2, 3] km and [2, 4] km, and the γ is 2 SSs/km^2. As we can see, the maximum CP is at the point where the tether length equals the middle value of the range of the uniform distribution. It is noteworthy that in some cases, there is actually a set of values of the tether length that can achieve this maximum value.

B. Two-Tier Network

In Fig. 6, CP of the two-tier network is shown, in which we also set three different values of $\tau = 0.1, 0.15, 0.2$, and compare the results of analysis and simulation. In Fig. 6, we can see that the performance trends of analysis and simulation are basically the same with small gaps due to interference approximations.

In order to have a more direct comparison with a single-tier network, in the following simulations, we will fix the densities of two tiers γ_1 and γ_2 both equal to 1 SSs/km^2, the sum of

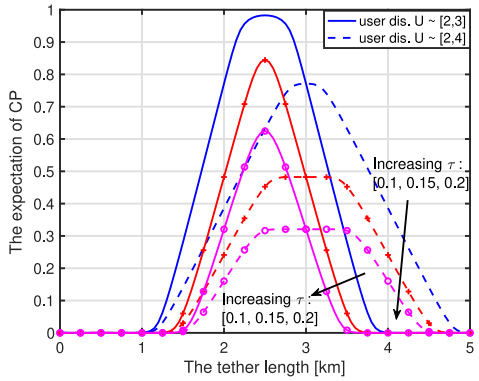

Fig. 5. Range and peak of CP in single-tier network with the distribution of UIoT device's depth are $U \sim [2, 3]$ km (solid lines) and $U \sim [2, 4]$ km (dashed lines), $\gamma = 2$ SSs/km^2.

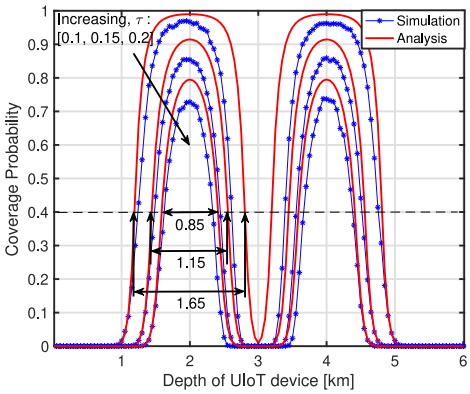

Fig. 6. CP of the two-tier network, under the situation that $\gamma_1 = \gamma_2 = 2$ SSs/km^2, $t_1 = 2$ km, $t_2 = 4$ km.

the two is equal to γ in a corresponding single-tier network and fixed the detection threshold $\tau = 0.2$. So in Fig. 7, we fixed $t_1 = 5$ km and then adjust t_2. In Fig. 7, we can find that based on the situation $t_1 = 5$ km, when t_2 is much shorter than, much longer than, or exactly equal to t_1, the peak has a high value. But when t_2 is equal to t_1, the range is very small. In this figure, we can find that if we have a two-tier network and want to have a bigger range and peak of CP, we need to make the distance difference between two tether lengths atleast 2 km.

Next, we explore the two-tier network's performance with a distribution instead of a given value of u_r. In order to compare the single-tier and the two-tier network performance, we will set the UIoT device's depth distribution as a uniform distribution over the range $[2, U_h]$ km, with U_h varying from 3 to 7 with the fixed $t_1 = 5$ km. Comparing the curve whose UIoT device depth is uniformly distributed over the range [2, 3] km in Fig. 8 and the same curve in Fig. 5, we can see that with the same range of uniform distribution of u_r, under the same detection threshold τ, the two-tiers network's performance is much better than the single-tier network, the peak of CP in Fig. 8 of $U \sim [2, 3]$ km is about 0.82 and the peak in Fig. 5 of $U \sim [2, 3]$ km is about 0.62.

In order to explore and uncover the best performance of a K-tier network, in Fig. 9, we exhibit the result of optimizing

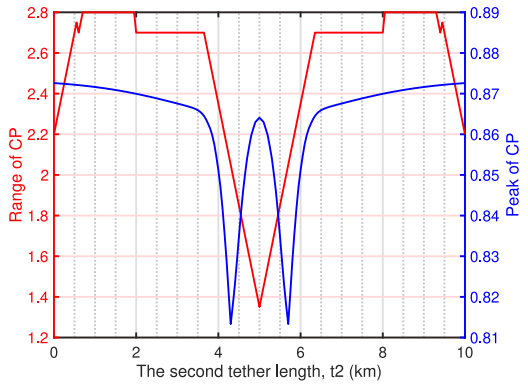

Fig. 7. CP of the two-tier network, $\gamma_1 = \gamma_2 = 1$ SSs/km^2, $\tau = 0.2$.

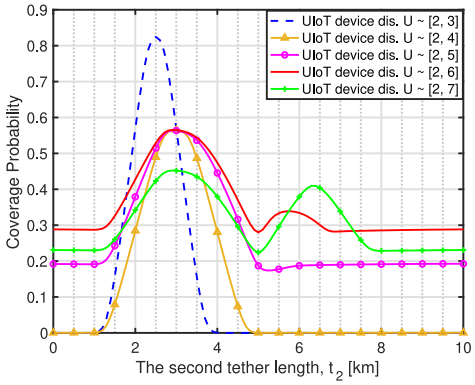

Fig. 8. Range and peak of CP in a two-tier network with $t_1 = 5$ km, $\gamma_1 = \gamma_2 = 1$ SSs/km^2, $\tau = 0.2$, and different distributions of UIoT device's depth.

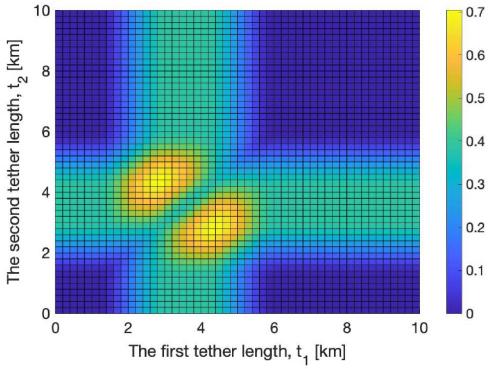

Fig. 9. Optimal two tether lengths in the two-tier network with $\gamma_1 = \gamma_2 = 1$ SSs/km^2, $\tau = 0.2$, and the distribution of UIoT device's depth is $U \sim [2,5]$ km.

two tether lengths in a two-tier network. In this simulation, we can achieve the biggest CP as 0.7032 at ($t_1 = 2.8$ km, $t_2 = 4.2$ km) or ($t_1 = 4.2$ km, $t_2 = 2.8$ km).

V. Conclusion and Further Work

UACNs are the backbone of underwater development and the prerequisite for the development of underwater multidevice collaboration. This raises the requirement of CP analysis of

UACNs. In this article, we developed a stochastic geometry-based model to study the performance of the CP and optimal CP under different application scenarios.

First, according to the hierarchical characteristics of underwater networks, we build a K-tier network. Next, we derived the CP of the UIoT device as a function of densities of PPPs, length of tiers' tether length, and other factors. Furthermore, we showed that the performance of the K-tier network can achieve better performance. In particular, we showed that under the background that the UIoT device has a small range of depth, a single-tier network is good, and with a large range of UIoT device's depth, a multitier network is better. In addition, we showed that the maximum CP can be achieved by optimizing the tether lengths of the different tiers.

This article is one of the few concrete works that symbiotically merge the randomness of the network geometry and the harsh environment of underwater acoustic communication.

Appendix A
Proof of Lemma 1

Since we already have the relationship between $D_{m,1}$ and $R_{m,1}$, we can derive the PDF of $R_{m,1}$ with given $r_{m,2}$ as follows:

$$\begin{aligned}
&F_{D_{m,1}}\left(d_{m,1}|r_{m,2}\right) = P\left(D_{m,1} \le d_{m,1}|r_{m,2}\right)\\
&= P\left(\sqrt{R_{m,1}^2 + (u_r - t_m)^2} \le d_{m,1}\middle|r_{m,2}\right)\\
&= P\left(0 \le R_{m,1} \le \sqrt{d_{m,1}^2 - (u_r - t_m)^2}\middle|r_{m,2}\right)\\
&= \begin{cases} \int_0^{\min\left(\sqrt{d_{m,1}^2-(u_r-t_m)^2},\ r_{m,2}\right)} \frac{2r_{m,1}}{r_{m,2}^2}\mathrm{d}r_{m,1} \\ \qquad\qquad \text{if } d_{m,1} > |u_r - t_m| \\ 0, \qquad\qquad \text{else} \end{cases}\\
&= \begin{cases} \frac{\left(\min\left(\sqrt{d_{m,1}^2-(u_r-t_m)^2}, r_{m,2}\right)\right)^2}{r_{m,2}^2}, \text{ if } d_{m,1} > |u_r - t_m| \\ 0, \qquad\qquad \text{else} \end{cases}\\
&= \frac{\left(\min\left(\sqrt{\max\left(d_{m,1}^2 - (u_r - t_m)^2, 0\right)}, r_{m,2}\right)\right)^2}{r_{m,2}^2}\\
&= \frac{\min\left(\max\left(d_{m,1}^2 - (u_r - t_m)^2, 0\right), r_{m,2}^2\right)}{r_{m,2}^2}
\end{aligned}$$

where u_r is the depth of the UIoT device which is given and t_m is the tether length of the mth tier which is known.

Appendix B
Proof of Lemma 2

$Y_{m,1}$ is the path loss of useful signal as shown in Definition 3, based on the relationship between $Y_{m,1}$ and $D_{m,1}$, added with PDF of $D_{m,1}$ in (28), we can derive the CDF of $Y_{m,1}$ as following:

$$\begin{aligned}
&F_{Y_{m,1}}\left(y_{m,1}|r_{m,2}\right) = P\left(Y_{m,1} \le y_{m,1}|r_{m,2}\right)\\
&= P\left(D_{m,1}^{-\lambda} 10^{-0.1\alpha D_{m,1}} \le y_{m,1}\middle|r_{m,2}\right)\\
&= P\left(D_{m,1} \ge \frac{10\lambda}{\alpha\ln(10)} W\left(\frac{\alpha\ln(10)}{10\lambda} y_{m,1}^{\frac{-1}{\lambda}}\right)\middle|r_{m,2}\right)\\
&= 1 - P\left(D_{m,1} \le \frac{10\lambda}{\alpha\ln(10)} W\left(\frac{\alpha\ln(10)}{10\lambda} y_{m,1}^{\frac{-1}{\lambda}}\right)\middle|r_{m,2}\right)\\
&= 1 - F_{D_{m,1}}\left(\frac{10\lambda}{\alpha\ln(10)} W\left(\frac{\alpha\ln(10)}{10\lambda} y_{m,1}^{\frac{-1}{\lambda}}\right)\middle|r_{m,2}\right)\\
&= 1 - \frac{\min\left(\max\left(\left(\frac{10\lambda}{\alpha\ln(10)} W\left(\frac{\alpha\ln(10)}{10\lambda} y_{m,1}^{\frac{-1}{\lambda}}\right)\right)^2 - (u_r - t_m)^2, 0\right), r_{m,2}^2\right)}{r_{m,2}^2}
\end{aligned}$$

where u_r and $r_{m,2}$ are given, t_m is known.

Appendix C
Proof of Lemma 3

When we calculate, in order to reduce the number of variables in a function, we divided intrainterference into the main interference which is created by the second SS in mth tier based on $r_{m,2}$

$$\begin{aligned}
&\mathbb{E}\left[I_{\text{Intra}-m3}\left(D_{m,i}|u_r\right)\right] = \mathbb{E}\left[\sum_{i=3} \frac{P_t}{C} Tl^{-1}\left(D_{m,i}|u_r\right)\right]\\
&= \frac{P_t}{C}\mathbb{E}\left[\sum_{i=3} D_{m,i}^{-\lambda} 10^{-0.1\alpha D_{m,i}}\right] = \frac{P_t}{C}\gamma_m \int_{\mathbb{R}^2} d_m^{-\lambda} 10^{-0.1\alpha d_m}\mathrm{d}d_m\\
&= \frac{P_t}{C}\gamma_m \int_{d_{m,2}}^{\infty}\int_0^{2\pi} d_m^{-\lambda} 10^{-0.1\alpha d_m}\mathrm{d}\theta\, d_m \mathrm{d}d_m\\
&= \frac{P_t}{C}\gamma_m 2\pi \int_{d_{m,2}}^{\infty} d_m^{1-\lambda} 10^{-0.1\alpha d_m}\mathrm{d}d_m\\
&= \frac{P_t}{C}\gamma_m 2\pi \int_{0.1\alpha d_{m,2}}^{\infty} \left(\frac{1}{0.1\alpha}\right)^{1-\lambda} (0.1\alpha d_m)^{1-\lambda} \frac{10^{-0.1\alpha d_m}}{0.1\alpha}\mathrm{d}(0.1\alpha d_m)\\
&= \frac{P_t}{C}\gamma_m 2\pi \left(\frac{1}{0.1\alpha}\right)^{2-\lambda} \int_{0.1\alpha d_{m,2}}^{\infty} (0.1\alpha d_m)^{1-\lambda} 10^{-0.1\alpha d_m}\mathrm{d}(0.1\alpha d_m)\\
&= \frac{P_t}{C}\gamma_m 2\pi \left(\frac{1}{0.1\alpha}\right)^{2-\lambda} \ln^{\lambda-2}(10)\Gamma\left(2-\lambda, \frac{\alpha d_{m,2}\ln(10)}{10}\right)
\end{aligned}$$

where $\Gamma(\cdot)$ is the Gamma function. So, we have the total intrainterference in the mth tier as shown in (34) which is based on the distance to the second nearest SS in the mth tier.

Appendix D
Proof of Lemma 4

Before we calculate the distribution of interinterference, we need to derive the distribution of main path loss which is created by the first closest distance in the jth tier. We already have the distribution of the first distance in jth tier as shown in (36) and the relationship between $D_{j,1}$ and $Y_{j,1}$, it is easy to derive the CDF of $Y_{j,1}$ as follows:

$$\begin{aligned}
&F_{Y_{j,1}}\left(y_{j,1}\right) = P\left(Y_{j,1} \le y_{j,1}\right) = P\left(D_{j,1}^{-\lambda} 10^{-0.1\alpha D_{j,1}} \le y_{j,1}\right)\\
&= P\left(D_{j,1} \ge \frac{10\lambda}{\alpha\ln(10)} W\left(\frac{\alpha\ln(10)}{10\lambda} y_{j,1}^{\frac{-1}{\lambda}}\right)\right)\\
&= 1 - P\left(z_j \le D_{j,1} \le \frac{10\lambda}{\alpha\ln(10)} W\left(\frac{\alpha\ln(10)}{10\lambda} y_{j,1}^{\frac{-1}{\lambda}}\right)\right)\\
&= 1 - \int_{z_j}^{\frac{10\lambda}{\alpha\ln(10)} W\left(\frac{\alpha\ln(10)}{10\lambda} y_{j,1}^{\frac{-1}{\lambda}}\right)} 2\pi\gamma_j d_{j,1} e^{-\gamma_m\pi\left(d_{j,1}^2 - z_j t^2\right)}\mathrm{d}d_{j,1}
\end{aligned}$$

$$= 1 - \left(- \exp\left(-\gamma_j \pi \left(d_{j,1}^2 - z_j^2\right)\right)\Big|_{d_{j,1}=z_j}^{d_{j,1}=\frac{10\lambda}{\alpha \ln(10)} W\left(\frac{\alpha \ln(10)}{10\lambda} y_{j,1}^{\frac{-1}{\lambda}}\right)} \right)$$

$$= \exp\left(-\gamma_j \pi \left(\left(\frac{10\lambda}{\alpha \ln(10)} W\left(\frac{\alpha \ln(10)}{10\lambda} y_{j,1}^{\frac{-1}{\lambda}}\right)\right)^2 - z_j^2\right)\right).$$

APPENDIX E
PROOF OF LEMMA 5

When we compute the interinterference, we divide it into two parts, one is the main interinterference which is made by the first closest SS in every tier except the mth, and another is the remaining interinterference whose expectation can be calculated approximately based on the first closest distance $d_{j,1}$

$$\mathbb{E}\left[I_{\text{Inter}-j2}\left(D_{j,i}|u_r\right)\right] = \mathbb{E}\left[\sum_{i=2}\left(\frac{P_t}{C} Tl^{-1}\left(D_{j,i}|u_R\right)\right)\right]$$

$$= \frac{P_t}{C}\mathbb{E}\left[\sum_{i=2}\left(D_{j,i}^{-\lambda} 10^{-0.1\alpha D_{j,i}}\right)\right] = \frac{P_t}{C}\gamma_j \int_{\mathbb{R}^2}\left(d_j^{-\lambda} 10^{-0.1\alpha d_j}\right)\mathrm{d}d_j$$

$$= \frac{P_t}{C}\gamma_j \int_{d_{j,1}}^{\infty}\int_0^{2\pi} d_j^{-\lambda} 10^{-0.1\alpha d_j} d_j \mathrm{d}\theta \mathrm{d}d_j$$

$$= \frac{P_t}{C}\gamma_j 2\pi \int_{d_{j,1}}^{\infty} d_j^{1-\lambda} 10^{-0.1\alpha d_j}\mathrm{d}d_j$$

$$= \frac{P_t}{C}\gamma_j 2\pi \int_{0.1\alpha d_{j,1}}^{\infty}\left(\frac{1}{0.1\alpha}\right)^{1-\lambda}\left(0.1\alpha d_j\right)^{1-\lambda} 10^{-0.1\alpha d_j}\frac{1}{0.1\alpha}\mathrm{d}\left(0.1\alpha d_j\right)$$

$$= \frac{P_t}{C}\gamma_j 2\pi \left(\frac{1}{0.1\alpha}\right)^{2-\lambda}\int_{0.1\alpha d_{j,1}}^{\infty}\left(0.1\alpha d_j\right)^{1-\lambda} 10^{-0.1\alpha d_j}\mathrm{d}\left(0.1\alpha d_j\right)$$

$$= \frac{P_t}{C}\gamma_j 2\pi \left(\frac{1}{0.1\alpha}\right)^{2-\lambda}\ln^{\lambda-2}(10)\Gamma\left(2-\lambda, \frac{\alpha d_{j,1}\ln(10)}{10}\right)$$

where, $d_{j,1}^2 = r_{j,1}^2 + (u_r - t_j)^2$, and u_r and t_j are given.

APPENDIX F
PROOF OF THEOREM 1

A_m is the probability that the useful signal or tagged SS appears in the mth tier. It means that we need to derive the probability that the closest SS in the mth tier will be closer than all nearest SS in every other tier. We can compare $D_{m,1}$ with $D_{j,1}$, for all j, respectively, as follows:

$$A_{m|u_r} = \prod_{\substack{j=1,\\ j\neq m}}^{j=k} P\left(|u_r - t_m| \le D_{m,1} \le D_{j,1}|u_r\right) = \prod_{\substack{j=1,\\ j\neq m}}^{j=k} F_{D_{m,1}}\left(D_{j,1}|u_r\right)$$

$$= \prod_{\substack{j=1,\\ j\neq m}}^{j=k} 1 - \exp\left(-\gamma_m \pi\left(\max\left(D_{j,1}^2, (u_r - t_m)^2\right) - (u_r - t_m)^2\right)\right)$$

$$= \prod_{\substack{j=1,\\ j\neq m}}^{j=k}\int f_{D_{j,1}}\left(d_{j,1}\right)\left(1 - e^{-\gamma_m \pi\left(\max\left(d_{j,1}^2, (u_r-t_m)^2\right) - (u_r-t_m)^2\right)}\right)\mathrm{d}d_{j,1}$$

$$= \prod_{\substack{j=1,\\ j\neq m}}^{j=k}\left(\int_{\sqrt{(u_r-t_j)^2}}^{\infty} 2\pi\gamma_j d_{j,1}\exp\left(-\gamma_j\pi\left(d_{j,1}^2 - \left(u_r - t_j\right)^2\right)\right)\mathrm{d}d_{j,1}\right.$$

$$- \int_{\sqrt{(u_r-t_j)^2}}^{\infty} 2\pi\gamma_j d_{j,1}\exp\left(-\gamma_j\pi\left(d_{j,1}^2 - \left(u_r - t_j\right)^2\right)\right.$$

$$\left.\left. - \gamma_m\pi\left(\max\left(d_{j,1}^2, (u_r - t_m)^2\right) - (u_r - t_m)^2\right)\right)\mathrm{d}d_{j,1}\right)$$

$$= \prod_{\substack{j=1,\\ j\neq m}}^{j=k}\left(\int_{\sqrt{(u_r-t_j)^2}}^{\infty} 2\pi\gamma_j d_{j,1}\exp\left(-\gamma_j\pi\left(d_{j,1}^2 - \left(u_r - t_j\right)^2\right)\right)\mathrm{d}d_{j,1}\right.$$

$$- \int_{\sqrt{(u_r-t_j)^2}}^{\infty} 2\pi\gamma_j d_{j,1}\exp\left(-\gamma_j\pi d_{j,1}^2\right.$$

$$\left.\left. - \gamma_m\pi\left(\max\left(d_{j,1}^2, (u_r - t_m)^2\right)\right)\right.\right.$$

$$\left.\left. + \gamma_j\pi\left(u_r - t_j\right)^2 + \gamma_m\pi\left(u_r - t_m\right)^2\right)\mathrm{d}d_{j,1}\right)$$

$$= \prod_{\substack{j=1,\\ j\neq m}}^{j=k}\left(-e^{-\gamma_j\pi\left(d_{j,1}^2 - (u_r-t_j)^2\right)}\Big|_{d_{j,1}=\sqrt{(u_r-t_j)^2}}^{d_{j,1}=\infty}\right.$$

$$+ \mathbb{1}\left(|u_r - t_m| < |u_r - t_j|\right)\frac{\gamma_j}{\gamma_j+\gamma_m}\exp\left(-d_{j,1}^2\pi\left(\gamma_j+\gamma_m\right)\right.$$

$$\left. + \gamma_j\pi\left(u_r - t_j\right)^2 + \gamma_m\pi\left(u_r - t_m\right)^2\right)\Big|_{d_{j,1}=\sqrt{(u_r-t_j)^2}}^{d_{j,1}=\infty}$$

$$+ \mathbb{1}\left(|u_r - t_j| \le |u_r - t_m|\right)$$

$$\times \exp\left(-\gamma_j\pi\left(d_{j,1}^2 - \left(u_r - t_j\right)^2\right)\right)\Big|_{d_{j,1}=\sqrt{(u_r-t_j)^2}}^{d_{j,1}=\sqrt{(u_r-t_m)^2}}$$

$$+ \mathbb{1}\left(|u_r - t_j| \le |u_r - t_m|\right)\frac{\gamma_j}{\gamma_j+\gamma_m}\exp\left(-d_{j,1}^2\pi\left(\gamma_j+\gamma_m\right)\right.$$

$$\left.\left. + \gamma_j\pi\left(u_r - t_j\right)^2 + \gamma_m\pi\left(u_r - t_m\right)^2\right)\Big|_{d_{j,1}=\sqrt{(u_r-t_m)^2}}^{d_{j,1}=\infty}\right)$$

$$= \prod_{\substack{j=1,\\ j\neq m}}^{j=k}\left(1 - \mathbb{1}\left(|u_r - t_m| < |u_r - t_j|\right)\frac{\gamma_j}{\gamma_j+\gamma_m}\right.$$

$$\times \exp\left(-\gamma_m\pi\left(u_r - t_j\right)^2 + \gamma_m\pi\left(u_r - t_m\right)^2\right)$$

$$+ \mathbb{1}\left(|u_r - t_j| \le |u_r - t_m|\right)$$

$$\times\left(\exp\left(-\gamma_j\pi\left(u_r - t_m\right)^2 + \gamma_j\pi\left(u_r - t_j\right)^2\right) - 1\right)$$

$$\left. - \mathbb{1}\left(|u_r - t_j| \le |u_r - t_m|\right)\frac{\gamma_j}{\gamma_j+\gamma_m}\right.$$

$$\left.\times \exp\left(-\gamma_j\pi\left(u_r - t_m\right)^2 + \gamma_j\pi\left(u_r - t_j\right)^2\right)\Big|u_r\right)$$

where, γ_m or γ_j are the densities of PPPs modeling the m-tier and j-tier, respectively, and u_r, t_m, and t_j are all given.

APPENDIX G
PROOF OF THEOREM 2

$$\mathbb{P}[\text{SINR}_m > \tau|u_r] = \mathbb{P}\left(\frac{P_r}{\sigma^2 + I_{\text{Intra}-m} + I_{\text{Inter}}} > \tau\left|u_r\right.\right)$$

$$= \mathbb{P}\left(\frac{P_t}{C}Tl^{-1}\left(D_{m,1}\right) > \tau\left(\sigma^2 + I_{\text{Intra}-m} + I_{\text{Inter}}\right)|u_r\right)$$

$$= \mathbb{P}\left(Tl^{-1}\left(D_{m,1}\right) > \tau\frac{C}{P_t}\left(\sigma^2 + I_{\text{Intra}-m} + I_{\text{Inter}}\right)|u_r\right)$$

$$= 1 - \mathbb{P}\left(Tl^{-1}\left(D_{m,1}\right) < \tau\frac{C}{P_t}\left(\sigma^2 + I_{\text{Intra}-m} + I_{\text{Inter}}\right)|u_r\right)$$

in order to compute the above probability, we define that

$$Y_{m,j} \triangleq \tau\frac{C}{P_t}\left(\sigma^2 + I_{\text{Intra}-m} + I_{\text{Inter}}\right). \tag{45}$$

According to (32)

$$\mathbb{P}[\mathrm{SINR}_m > \tau | u_r] = \int_{R_{m,2}} \int_{R_{1,1}} \int_{R_{2,1}} \cdots \int_{R_{k,1}} \left(1 - F_{Y_{m,1}}\left(y_{m,j} | r_{m,2}\right)\right) f\left(r_{1,1}\right) \times f\left(r_{2,1}\right) \cdots f\left(r_{k,1}\right) f\left(r_{m,2}\right) \mathrm{d}r_{1,1} \mathrm{d}r_{2,1} \cdots \mathrm{d}r_{k,1} \mathrm{d}r_{m,2}$$

and where

$$1 - F_{Y_{m,1}}\left(y_{m,j} | r_{m,2}\right) = \frac{\left(\min\left(\sqrt{\max\left(\left(\frac{10\lambda}{\alpha \ln(10)} W\left(\frac{\alpha \ln(10)}{10\lambda} y_{m,j}^{\frac{-1}{\lambda}}\right)\right)^2 - (u_r - t_m)^2, 0\right)}, r_{m,2}\right)\right)^2}{r_{m,2}^2}.$$

REFERENCES

[1] Y. Huo, X. Dong, and S. Beatty, "Cellular communications in ocean waves for maritime Internet of Things," *IEEE Internet Things J.*, vol. 7, no. 10, pp. 9965–9979, Oct. 2020.

[2] P. W. Kimball and S. M. Rock, "Mapping of translating, rotating icebergs with an autonomous underwater vehicle," *IEEE J. Ocean. Eng.*, vol. 40, no. 1, pp. 196–208, Jan. 2015.

[3] H. Ghafoor and Y. Noh, "An overview of next-generation underwater target detection and tracking: An integrated underwater architecture," *IEEE Access*, vol. 7, pp. 98841–98853, 2019.

[4] Q. Wang, H.-N. Dai, Q. Wang, M. K. Shukla, W. Zhang, and C. G. Soares, "On connectivity of UAV-assisted data acquisition for underwater Internet of Things," *IEEE Internet Things J.*, vol. 7, no. 6, pp. 5371–5385, Jun. 2020.

[5] J. Yang, J. Wen, Y. Wang, B. Jiang, H. Wang, and H. Song, "Fog-based marine environmental information monitoring toward ocean of things," *IEEE Internet Things J.*, vol. 7, no. 5, pp. 4238–4247, May 2020.

[6] A. Caiti *et al.*, "Linking acoustic communications and network performance: Integration and experimentation of an underwater acoustic network," *IEEE J. Ocean. Eng.*, vol. 38, no. 4, pp. 758–771, Oct. 2013.

[7] R. Diamant *et al.*, "On the relationship between the underwater acoustic and optical channels," *IEEE Trans. Wireless Commun.*, vol. 16, no. 12, pp. 8037–8051, Dec. 2017.

[8] E. M. Sozer, M. Stojanovic, and J. G. Proakis, "Underwater acoustic networks," *IEEE J. Ocean. Eng.*, vol. 25, no. 1, pp. 72–83, Jan. 2000.

[9] H. Kaushal and G. Kaddoum, "Underwater optical wireless communication," *IEEE Access*, vol. 4, pp. 1518–1547, 2016.

[10] W. Yu, Y. Chen, L. Wan, X. Zhang, P. Zhu, and X. Xu, "An energy optimization clustering scheme for multi-hop underwater acoustic cooperative sensor networks," *IEEE Access*, vol. 8, pp. 89171–89184, 2020.

[11] S. Zhang, K. Chen, Z. Fan, E. Cheng, and W. Su, "The localization algorithm based on symmetry correction for underwater acoustic networks," *IEEE Access*, vol. 7, pp. 121127–121135, 2019.

[12] P. S. Rossi, D. Ciuonzo, T. Ekman, and H. Dong, "Energy detection for MIMO decision fusion in underwater sensor networks," *IEEE Sensors J.*, vol. 15, no. 3, pp. 1630–1640, Mar. 2015.

[13] I. Ullah, J. Chen, X. Su, C. Esposito, and C. Choi, "Localization and detection of targets in underwater wireless sensor using distance and angle based algorithms," *IEEE Access*, vol. 7, pp. 45693–45704, 2019.

[14] Z. Lv, J. Zhang, J. Jin, and L. Liu, "Link strength for unmanned surface vehicle's underwater acoustic communication," in *Proc. IEEE/OES China Ocean Acoust. (COA)*, 2016, pp. 1–4.

[15] E. Cheng, L. Wu, F. Yuan, C. Gao, and J. Yi, "Node selection algorithm for underwater acoustic sensor network based on particle swarm optimization," *IEEE Access*, vol. 7, pp. 164429–164443, 2019.

[16] N. Morozs, P. D. Mitchell, and R. Diamant, "Scalable adaptive networking for the Internet of underwater things," *IEEE Internet Things J.*, vol. 7, no. 10, pp. 10023–10037, Oct. 2020.

[17] Z. Jin, Z. Ji, Y. Su, S. Li, and B. Wei, "A deployment optimization mechanism using depth adjustable nodes in underwater acoustic sensor networks," in *Proc. OCEANS MTS/IEEE Kobe Techno-Oceans (OTO)*, 2018, pp. 1–6.

[18] Y. Su, L. Guo, Z. Jin, and X. Fu, "A voronoi-based optimized depth adjustment deployment scheme for underwater acoustic sensor networks," *IEEE Sensors J.*, vol. 20, no. 22, pp. 13849–13860, Nov. 2020.

[19] Y. Ma *et al.*, "A quick deployment method for sonar buoy detection under the overview situation of underwater cluster targets," *IEEE Access*, vol. 8, pp. 11–25, 2020.

[20] Y. Deng, L. Wang, M. Elkashlan, A. Nallanathan, and R. K. Mallik, "Physical layer security in three-tier wireless sensor networks: A stochastic geometry approach," *IEEE Trans. Inf. Forensics Security*, vol. 11, pp. 1128–1138, 2016.

[21] E. Chu, J. M. Kim, and B. C. Jung, "Interference analysis of directional UAV networks: A stochastic geometry approach," in *Proc. 11th Int. Conf. Ubiquitous Future Netw. (ICUFN)*, 2019, pp. 9–12.

[22] O. A. Amodu, M. Othman, N. K. Noordin, and I. Ahmad, "Relay-assisted D2D underlay cellular network analysis using stochastic geometry: Overview and future directions," *IEEE Access*, vol. 7, pp. 115023–115051, 2019.

[23] X. Li and D. Zhao, "Capacity research in cluster-based underwater wireless sensor networks based on stochastic geometry," *China Commun.*, vol. 14, no. 6, pp. 80–87, 2017.

[24] Q. Wang, H.-N. Dai, C. F. Cheang, and H. Wang, "Link connectivity and coverage of underwater cognitive acoustic networks under spectrum constraint," *Sensors*, vol. 17, no. 12, p. 2839, 2017.

[25] T. Qiu, Z. Zhao, T. Zhang, C. Chen, and C. L. P. Chen, "Underwater Internet of Things in smart ocean: System architecture and open issues," *IEEE Trans. Ind. Informat.*, vol. 16, no. 7, pp. 4297–4307, Jul. 2020.

[26] M. A. Abd-Elmagid, M. A. Kishk, and H. S. Dhillon, "Joint energy and SINR coverage in spatially clustered RF-powered IoT network," *IEEE Trans. Green Commun. Netw.*, vol. 3, no. 1, pp. 132–146, Mar. 2019.

[27] M. A. Kishk and H. S. Dhillon, "Joint uplink and downlink coverage analysis of cellular-based RF-powered IoT network," *IEEE Trans. Green Commun. Netw.*, vol. 2, no. 2, pp. 446–459, Jun. 2018.

[28] R. J. Urick, *Principles of Underwater Sound-2*. New York, NY, USA: McGraw-Hill, 1975.

[29] M. Stojanovic, "On the relationship between capacity and distance in an underwater acoustic communication channel," *ACM SIGMOBILE Mobile Comput. Commun. Rev.*, vol. 11, no. 4, pp. 34–43, 2007.

[30] M. Stojanovic and J. Preisig, "Underwater acoustic communication channels: Propagation models and statistical characterization," *IEEE Commun. Mag.*, vol. 47, no. 1, pp. 84–89, Jan. 2009.

[31] J.-G. Huang, H. Wang, C.-B. He, Q.-F. Zhang, and L.-Y. Jing, "Underwater acoustic communication and the general performance evaluation criteria," *Front. Inf. Technol. Electron. Eng.*, vol. 19, no. 8, pp. 951–971, 2018.

[32] N. Saeed, A. Celik, T. Y. Al-Naffouri, and M.-S. Alouini, "Energy harvesting hybrid acoustic-optical underwater wireless sensor networks localization," *Sensors*, vol. 18, no. 1, p. 51, 2018.

[33] J. G. Andrews, A. K. Gupta, and H. S. Dhillon, "A primer on cellular network analysis using stochastic geometry," 2016, *arXiv:1604.03183*.

[34] D. Moltchanov, "Distance distributions in random networks," *Ad Hoc Netw.*, vol. 10, pp. 1146–1166, Aug. 2012.

Jiajie Xu (Student Member, IEEE) received the B.Sc. degree from Lanzhou Jiaotong University, Lanzhou, China, in 2016, and the M.Sc. degree from Yanshan University, Qinhuangdao, China, in 2019. He is currently pursuing the Ph.D. degree with the Communication Theory Laboratory, King Abdullah University of Science and Technology, Thuwal, Saudi Arabia.

His current research interests include underwater wireless acoustic communication, underwater target detection, underwater cooperative networks, maritime communication, space–air–ground–sea integrated communication system and joint sensing and communication system, stochastic geometry, and energy harvesting wireless networks.

Mustafa A. Kishk (Member, IEEE) received the B.Sc. and M.Sc. degrees from Cairo University, Giza, Egypt, in 2013 and 2015, respectively, and the Ph.D. degree from Virginia Tech, Blacksburg, VA, USA, in 2018.

He is an Assistant Professor with the Electronic Engineering Department, Maynooth University, Maynooth, Ireland. Before that, he was a Postdoctoral Research Fellow with the Communication Theory Laboratory, King Abdullah University of Science and Technology, Thuwal, Saudi Arabia. His current research interests include stochastic geometry, energy harvesting wireless networks, UAV-enabled communication systems, and satellite communications.

Mohamed-Slim Alouini (Fellow, IEEE) was born in Tunis, Tunisia. He received the Ph.D. degree in electrical engineering from California Institute of Technology, Pasadena, CA, USA, in 1998.

He served as a Faculty Member with the University of Minnesota, Minneapolis, MN, USA, then with Texas A&M University at Qatar, Doha, Qatar, before joining in 2009 the King Abdullah University of Science and Technology, Thuwal, Saudi Arabia, where he is currently a Distinguished Professor of Electrical and Computer Engineering. He is currently particularly interested in addressing the technical challenges associated with the uneven distribution, access to, and use of information and communication technologies in far-flung, rural, low-density populations, low-income, and/or hard-to-reach areas.

Prof. Alouini is a Fellow of OSA.